https://doi.org/10.5194/egusphere-2026-3545
Preprint. Discussion started: 3 August 2026

1D-VAR system for a ground-based microwave radiometer: application of an inter-channel observation-error covariance matrix

Yunyoung Song[1], Myoung-Hwan Ahn[1*], Su Jeong Lee[1], Domenico Cimini[2,3], Chang-Keun Song[4,5,6]

[1]Department of Climate and Energy Systems Engineering, Ewha Womans University, Seoul, 03760, Republic of Korea
[2]National Research Council of Italy, Institute of Methodologies for Environmental Analysis, Potenza, 85050, Italy
[3]Center of Excellence CETEMPS, University of L'Aquila, L'Aquila, 67100, Italy
[4]Department of Civil, Urban, Earth, and Environmental Engineering, Ulsan National Institute of Science and Technology, Ulsan 44919, South Korea
[5]Graduate School of Carbon Neutrality, Ulsan National Institute of Science and Technology (UNIST), Ulsan 44919, South Korea
[6]Research & Management Center for Particulate Matters at the Southeast Region of Korea, Ulsan National Institute of Science and Technology (UNIST), Ulsan 44919, South Korea

Correspondence to: Myoung-Hwan Ahn (terryahn65@ewha.ac.kr)

Abstract. This study presents the specification of an inter-channel observation-error covariance matrix (**R**) and evaluates its effects on One-Dimensional Variational (1D-VAR) retrievals from a ground-based microwave radiometer (MWR) using RTTOV-gb as the observation operator. In the 1D-VAR, the accurate characterization of the background error covariance matrix and **R** is crucial, as they determine the relative weighting of background and observational uncertainties and thus directly control retrieval performance. However, realistic specification of **R** remains challenging due to the complexity of error sources, including instrument noise, forward-model error, and representativeness error. Consequently, many previous studies have adopted a simplified diagonal approximation. In this study, a correlated **R** is specified and compared with its diagonal configuration to quantify the effects of inter-channel error correlations on 1D-VAR performance. Radiosonde validation shows root mean square error (RMSE) reductions of 1.02 % for temperature and 4.52 % for humidity relative to the diagonal configuration below 1000 m. Using the correlated configuration, the 1D-VAR retrieval outperforms the Numerical Weather Prediction (NWP) model used as the background in the lowest 1000 m, achieving RMSE reductions of up to 23 % for temperature and 12 % for humidity, indicating an improved representation of near-surface variability during the intensive observation periods. The correlated configuration improves convergence efficiency, with 5.7 % of successful retrievals converging in a single iteration (compared to 0.1 % for the diagonal configuration), reducing the total processing time by approximately 2.6 %. In addition to enhanced computational efficiency, the correlated **R** maintains comparable retrieval accuracy in the lower troposphere. Overall, explicitly accounting for inter-channel observation-error correlations enhances convergence efficiency and provides modest improvements in retrieval accuracy below 1000 m, highlighting the importance of realistic observation-error covariance specification for lower-tropospheric thermodynamic profiling.

https://doi.org/10.5194/egusphere-2026-3545
Preprint. Discussion started: 3 August 2026

1 Introduction

To characterize rapid thermodynamic variability in the boundary layer, high-accuracy, high-resolution atmospheric profiles are essential. However, Numerical Weather Prediction (NWP) models often struggle to capture boundary-layer processes on short timescales because of strong interactions with the underlying surface (Calaf et al., 2023; Powers et al., 2017). Ground-based Microwave Radiometers (MWRs) are advantageous for monitoring thermodynamic variability in the boundary layer. Most of the brightness temperature (TB) information used to retrieve temperature profiles is concentrated in the boundary layer (Löhnert and Maier, 2012). Moreover, MWRs measure atmospheric emissions every few seconds, and their unattended, long-term operation makes them well-suited for continuous monitoring.

For these reasons, previous studies have used MWR observations in One-Dimensional Variational (1D-VAR) retrievals as a preliminary step toward integration into data assimilation systems. The efficacy of MWR-based 1D-VAR retrievals has been demonstrated across various mesoscale and convective-scale models (Cimini et al., 2010, 2011; Hewison, 2007; Martinet et al., 2015, 2017, 2022). More recently, direct assimilation experiments using MWR observations in 3D/4D-VAR have been conducted in a limited number of studies. These studies have reported improvements in boundary layer analyses and forecasts of extreme weather (Ikuta et al., 2025; Thomas et al., 2025; Vural et al., 2024; Zheng et al., 2026).

In the cost function of 1D-VAR retrieval and variational data assimilation, the observation-error covariance matrix represents observation uncertainties, and thus retrieval performance depends on how realistically these error statistics are specified. Since an accurate estimate of the full observation-error covariance matrix in practice is difficult, a diagonal observation-error covariance matrix has traditionally been used, assuming that observation errors are uncorrelated.

However, remote sensing observations usually have correlated errors. Previous studies have shown that accounting for inter-channel correlations in 1D-VAR retrieval and data assimilation increases the effective use of observational information and improves analysis accuracy (Hu and Dance, 2024; Stewart et al., 2008, 2013; Weston et al., 2014). Ikuta et al. (2025) also reported the presence of inter-channel error correlations in MWR observations and demonstrated that accounting for these correlations improves precipitation forecast in NWP.

To account for correlations indirectly, observation-error variances are inflated, but this approximation can degrade performance compared with explicitly representing the true correlations (Stewart et al., 2008, 2013; Weston et al., 2014). Meanwhile, the diagnostic method proposed by Desroziers et al. (2005) is widely used to estimate observation-error statistics, including error correlations. However, it has been pointed out that this method is vulnerable to bias and noise (Hu and Dance, 2024; Ikuta et al., 2025). Therefore, a realistic representation of observation-error covariances in MWR-based 1D-VAR retrieval requires physically based characterization of error components (e.g., instrument, forward model, and representativeness errors), statistically representative estimation using bias-corrected MWR observations, and explicit treatment of inter-channel error correlations to reduce noise-induced uncertainties.

In this study, we implemented a 1D-VAR system utilizing MWR observations with the Local Data Assimilation and Prediction System (LDAPS), a high-resolution (1.5 km) regional-scale NWP model, under clear-sky conditions. The observation-error

https://doi.org/10.5194/egusphere-2026-3545
Preprint. Discussion started: 3 August 2026

covariance matrix is estimated to account for inter-channel error correlations using samples obtained from bias-corrected MWR observations.

Because few studies have directly compared a correlated (FULL) covariance matrix with a diagonal matrix within the same 1D-VAR framework, we perform a direct comparison between a FULL matrix and its diagonal counterpart, obtained by setting all off-diagonal elements to zero. By comparing these two configurations, we quantify the impact of accounting for inter-channel error correlations on the vertical structure of retrieved profiles and the convergence efficiency. This paper begins with an overview of the datasets and preprocessing steps required for implementing the algorithm (Sect. 2). It then describes the 1D-VAR configuration and specifies the observation-error covariance matrix accounting for inter-channel error correlations (Sect. 3). Section 4 evaluates the retrieval performance and compares retrievals using an observation-error covariance matrix with only diagonal components. Finally, Section 5 summarizes the main conclusions.

2 DATA

2.1 Ground-based Microwave radiometer (MWR)

The fourth-generation Humidity And Temperature PROfiler (HATPRO) MWR, manufactured by Radiometer Physics GmbH, measures downwelling microwave radiation within a frequency range of 22–58 GHz. In this study, TB data were collected from 14 channels of the HATPRO MWR deployed at the Jungnang site in Seoul (Fig. 1, 37.59° N, 127.07° E, 37 m above m.s.l.) during 2015–2016, excluding the summer of 2015 when the instrument experienced malfunction. HATPRO operates in two spectral ranges. The K-band channels (22.24, 23.04, 23.84, 25.44, 26.24, 27.84, and 31.40 GHz) are primarily sensitive to atmospheric humidity and cloud liquid water. In particular, the 22.24 GHz, located near the water vapor absorption line, can capture contributions from higher altitudes because the atmosphere is relatively optically thin at this frequency. In contrast, the V-band channels (51.26, 52.28, 53.86, 54.94, 56.66, 57.30, and 58.00 GHz) mainly provide temperature information. As the frequency approaches the center of the oxygen absorption complex near 60 GHz, the atmosphere becomes optically thicker, reducing the contribution from higher altitudes. Consequently, the increased atmospheric emission near the surface predominantly represents lower atmospheric information (Hewison, 2007; Martinet et al., 2015). The electromagnetic power signals received from microwave radiation are converted into TBs using calibration coefficients. Therefore, calibration is a crucial step to ensure accurate TB observations (Cimini et al., 2003; Martinet et al., 2017). In this study, liquid nitrogen (LN_2) calibration was performed twice during the considered period. Previous studies have shown that low-elevation angle observations can improve the accuracy of lower atmospheric temperature retrievals (Martinet et al., 2015). Multi-angle scans were not available at sufficiently high temporal frequency during these periods. Accordingly, this study focuses on developing the 1D-VAR system and utilizes only zenith angle observations.

https://doi.org/10.5194/egusphere-2026-3545
Preprint. Discussion started: 3 August 2026

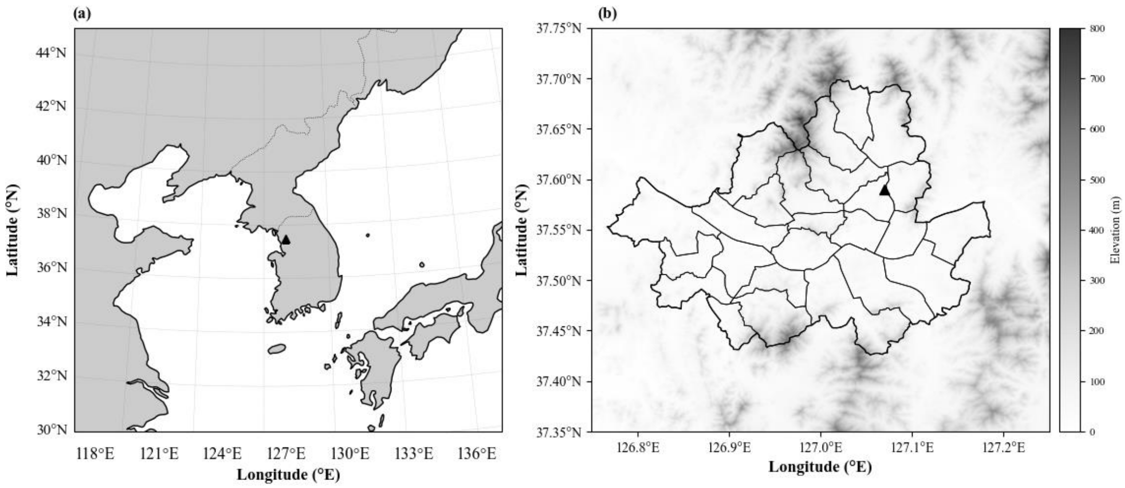

Figure 1: Location of the Jungnang site (triangle) in (a) East Asia and (b) the Seoul metropolitan area, with topography shown in (b).

2.2 Validation data

To validate the performance of the 1D-VAR algorithm, radiosondes were used. Radiosondes were launched during two intensive observation periods (IOPs) at the HATPRO site. The first IOP took place from 23 to 30 November 2015, with launches conducted every three hours at 00:00, 03:00, 06:00, 09:00, 12:00, 15:00, 18:00, and 21:00 UTC (56 observations in total). The second IOP occurred from 19 September to 7 October 2016, also with launches conducted every three hours (82 observations in total).

2.3 Quality control

2.3.1 Data screening

Before using the HATPRO MWR observations, a data screening procedure was applied to select clear-sky conditions. First, measurements flagged by the HATPRO MWR rain sensor were excluded from the analysis. The remaining data were then refined using a two-stage screening approach.

In the first stage, a cloud detection algorithm (Ahn et al., 2015) was applied to avoid additional uncertainty caused by clouds. The algorithm uses an Infrared Radiometer (IRT; 10.5 μm) installed on top of the HATPRO MWR and identifies clouds based on increases in TB measured by the IRT and on its temporal variability under cloudy conditions.

In the second stage, assuming reduced atmospheric variability under clear-sky conditions, samples were selected when the 10-min standard deviation (STD) of TB at 31.4 GHz (a cloud-sensitive window channel) was below 0.2 K (Cimini et al., 2019). As a result, 63 087 samples (57 %) were retained out of a total of 111 240 observations.

https://doi.org/10.5194/egusphere-2026-3545
Preprint. Discussion started: 3 August 2026

2.3.2 Observation minus background monitoring

The 1D-VAR retrieval assumes that observations are unbiased and that observation errors follow a Gaussian distribution. Because degraded observational quality can reduce the retrieval performance, quality control (QC) based on the characteristics of observation minus background departures (O–B) is commonly applied prior to 1D-VAR retrievals (Ebell et al., 2017; Löhnert and Maier, 2012; Martinet et al., 2015, 2017). MWR observations can be affected by Radio Frequency Interference, non-meteorological disturbances (e.g., the Sun, the Moon, humans, birds, aircraft, etc.), and calibration-related issues. These effects may appear as spikes or discontinuities in O–B time series, helping to identify potential error sources (instrument, observation operator, or a NWP model).

Figure 2 shows the observed TB and simulated TB using LDAPS at 22.24 GHz (a) and 51.26 GHz (d), and the corresponding O–B time series in (b) and (e), respectively. Panels (b) and (c) show the O–B time series before and after QC under clear-sky conditions. Two LN_2 calibrations were performed in September 2015 and September 2016, indicated by vertical dashed lines. Step-like changes are evident after both calibration events, particularly in the more transparent channels (Fig. 2e). The O–B shifted by –2.7 K after the first calibration and by –13.2 K after the second calibration at 51.26 GHz. Similar post-calibration discontinuities have been reported previously and may be associated with water condensation on the aluminum plate reflector and radiometer radome, as well as a non-uniform LN_2 coverage of the absorber (Löhnert and Maier, 2012). The magnitude of these effects depends on channel characteristics. Transparent channels located on the steep shoulder of the O_2 absorption complex are more sensitive to uncertainties in bandpass characterization and can therefore exhibit larger O–B differences. Additionally, contributions may also arise from absorption model uncertainties (Cimini et al., 2018), as well as other systematic uncertainties related to calibration. In contrast, opaque channels (54–58 GHz) typically show smaller discontinuities, consistent with typical values close to ambient temperature.

Although observation uncertainties are incorporated into the observation-error covariance matrix, systematic errors are not accounted for, which can potentially introduce bias and lead to non-convergence issues in retrievals. Therefore, for the V-band channels, a bias correction procedure was applied following Hewison et al. (2013). This method estimates fitting coefficients between observed and simulated TB using LDAPS separately for each data subset defined by LN_2 calibration events and applies the following relationships:

$$\mathrm{TB\ (MWR)} = \mathrm{C}_0 + \mathrm{C}_1 \times \mathrm{TB\ (simulated)},$$

$$\mathrm{TB}\left(\mathrm{MWR}_{\mathrm{bias\_corrected}}\right) = \frac{(\mathrm{TB\ (MWR)} - \mathrm{C}_0)}{\mathrm{C}_1}. \quad (1)$$

In addition, outliers exceeding 3 STD from the mean O–B differences were removed. The final QC results are shown in Fig. 2c, f. After the bias correction, the systematic component was substantially reduced. The resulting observations were used in the 1D-VAR retrieval, supporting the assumptions underlying the method.

https://doi.org/10.5194/egusphere-2026-3545
Preprint. Discussion started: 3 August 2026

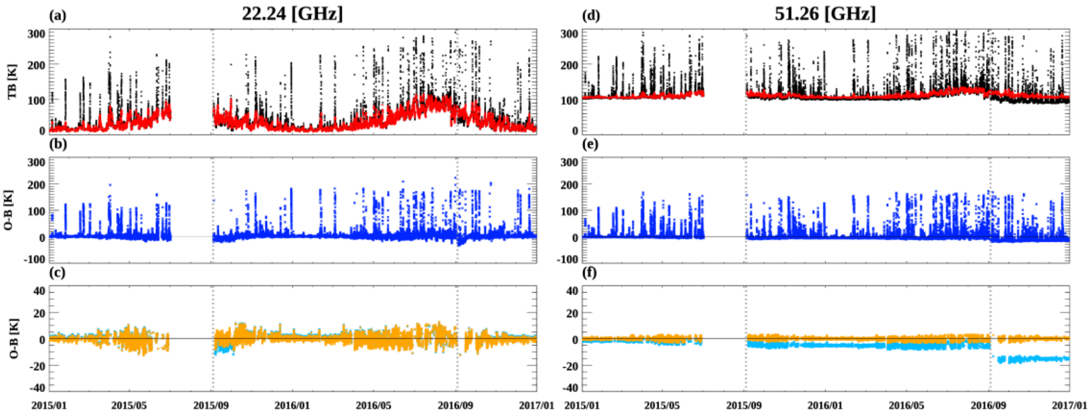

Figure 2: Time series of observed brightness temperatures (TB) and TB simulated from the NWP background, and their differences (O–B) for 22.24 GHz (a-c) and 51.26 GHz (d-f). (a, d) observed TB (black) and simulated TB (red); (b, e) O–B time series; and (c, f) O–B under clear-sky conditions (sky blue) and after quality control (gold).

3 Retrieval algorithm

3.1 1D-VAR framework

The 1D-VAR algorithm for MWR observations is based on Bayesian optimal estimation theory, which combines MWR observations with a priori information from an NWP model. The algorithm iteratively determines the atmospheric state vector $\boldsymbol{x}$ that best reproduces the observations $\boldsymbol{y}$. The solution is obtained by minimizing the following cost function $J(\boldsymbol{x})$:

$$J(\boldsymbol{x}) = [\boldsymbol{x} - \boldsymbol{x}_\mathrm{a}]^\mathrm{T}\mathbf{B}^{-1}[\boldsymbol{x} - \boldsymbol{x}_\mathrm{a}] + [\boldsymbol{y} - \boldsymbol{H}(\boldsymbol{x})]^\mathrm{T}\mathbf{R}^{-1}[\boldsymbol{y} - \mathbf{H}(\boldsymbol{x})], \tag{2}$$

where $\boldsymbol{x}_\mathrm{a}$ is the *a priori* state vector obtained from the LDAPS background fields, $\boldsymbol{H}(\boldsymbol{x})$ is the forward model implemented using RTTOV-gb (De Angelis et al., 2016), $\mathbf{B}$ is the background-error covariance matrix, $\mathbf{R}$ is the observation-error covariance matrix, $(\cdot)^T$ denotes the transpose operator, and $(\cdot)^{-1}$ indicates the inverse operator. During the minimization, the Gauss-Newton method (Rodgers, 2000) is applied to iteratively update the optimal solution from the state vector at iteration n, as:

$$\boldsymbol{x}_{n+1} = \boldsymbol{x}_\mathrm{a} + \mathbf{B}\mathbf{K}_n^\mathrm{T}(\mathbf{K}_n\mathbf{B}\mathbf{K}_n^\mathrm{T} + \mathbf{R})^{-1}[(\boldsymbol{y} - \boldsymbol{H}(\boldsymbol{x}_n)) + \mathbf{K}_\mathrm{n}(\boldsymbol{x}_n - \boldsymbol{x}_\mathrm{a})]. \tag{3}$$

The Jacobian matrix $\mathbf{K}_n$ represents the sensitivity of simulated TBs to changes in the state vector $\boldsymbol{x}$ and is computed using the K-module of RTTOV-gb. In this study, $\boldsymbol{x}_\mathrm{a}$ is taken from LDAPS, $\boldsymbol{y}$ denotes the observed TBs from the 14 MWR channels. The algorithm flowchart is shown in Fig. 3. Initially, if the mean RMSE between the observed TBs and the simulated TBs from the background state vector is below a threshold of 0.4 K, the background profile is directly chosen as the solution, and the algorithm terminates. The threshold was empirically selected from the O–B RMSE distribution derived from the quality-controlled TBs. If the mean RMSE exceeds this threshold, the state vector is iteratively updated to find an optimal solution, with a maximum of 10 iterations. Convergence is evaluated using two criteria. First, the step size in measurement space between successive iterations is evaluated using the observation dimension ($m = 14$) proposed by Rodgers (2000). However,

https://doi.org/10.5194/egusphere-2026-3545
Preprint. Discussion started: 3 August 2026

to reduce premature convergence, an effective observation dimension, $m_{\mathrm{eff}} = m/2$ is adopted (Hewison, 2006) and the following criterion is tested:

$$[\boldsymbol{H}(\boldsymbol{x}_{n+1}) - \boldsymbol{H}(\boldsymbol{x}_n)]^{\mathrm{T}}\, \mathbf{S}_{\delta\hat{y}}{}^{-1}[\boldsymbol{H}(\boldsymbol{x}_{n+1}) - \boldsymbol{H}(\boldsymbol{x}_n)] \ll m_{\mathrm{eff}}, \tag{4}$$

where $\mathbf{S}_{\delta\hat{y}}$ is given by

$$\mathbf{S}_{\delta\hat{y}} = \mathbf{R}(\mathbf{K}_n\mathbf{B}\mathbf{K}_n^{\mathrm{T}} + \mathbf{R})^{-1}\mathbf{R}\,. \tag{5}$$

If this condition is satisfied, a second test is conducted to evaluate the statistical consistency of the retrieval using a chi-square test $(\mathcal{X}^2)$. The $\mathcal{X}^2$ statistic is defined as

$$\mathcal{X}^2 = [\boldsymbol{H}(\boldsymbol{x}_{\mathrm{ret}}) - \boldsymbol{y}]^{\mathrm{T}}\, \mathbf{R}^{-1}[\boldsymbol{H}(\boldsymbol{x}_{\mathrm{ret}}) - \boldsymbol{y}]. \tag{6}$$

Here, $\boldsymbol{x}_{\mathrm{ret}}$ represents the retrieved profile at the convergence step. A retrieval is considered successful when $\mathcal{X}^2$ is below a predefined threshold of 100, following Hewison (2007). This threshold was found to provide a reasonable balance between retrieval convergence and retrieval performance in this study.

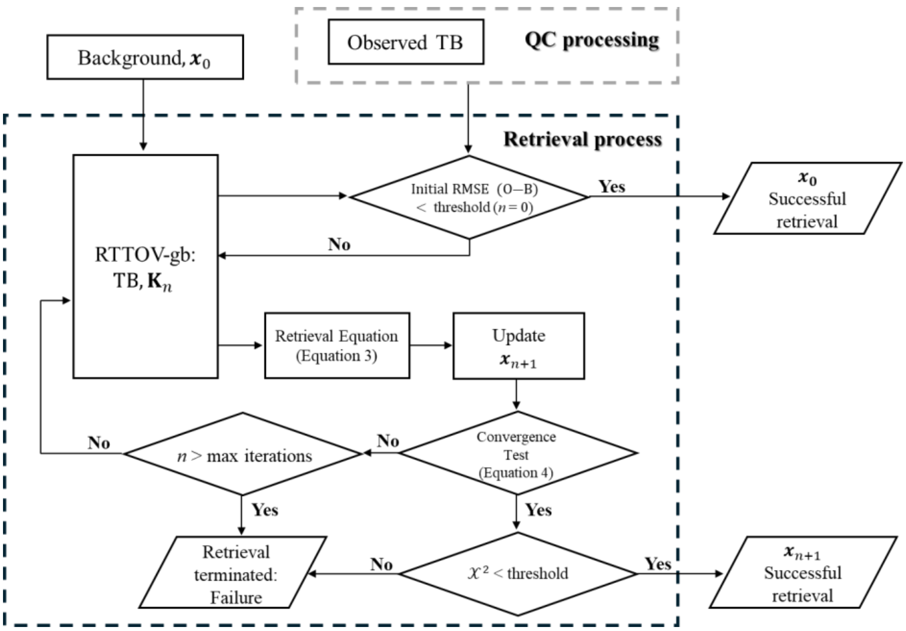

Figure 3: 1D-VAR algorithm flowchart.

3.2 NWP model

In this study, LDAPS forecasts are used as a priori (background) profiles for the 1D-VAR retrievals. LDAPS, developed by the Korea Meteorological Administration (KMA) based on the Unified Model (UM), serves as a local-scale data assimilation and prediction system. Previous studies have reported that LDAPS shows good skill for near-surface (lower-tropospheric) variables (Kang et al., 2015) and can capture urban meteorological features relevant to local forecasting (Byon et al., 2021). LDAPS is operated on a high-resolution grid to mitigate weather-related disasters associated with severe weather events over

https://doi.org/10.5194/egusphere-2026-3545
Preprint. Discussion started: 3 August 2026

the Korean Peninsula (Kim et al., 2020). The horizontal grid comprises 602 × 781 points with a spatial resolution of 1.5 km, and the vertical grid consists of 70 levels extending to approximately 40 km above the surface. LDAPS runs eight times per day: four main cycles (00, 06, 12, and 18 UTC) produce forecasts up to 36 h, and the other four additional cycles (03, 09, 15, and 21 UTC) produce short-range forecasts up to 3 h. It employs a three-dimensional variational (3D-VAR) data assimilation scheme and receives lateral boundary conditions from the global model every three hours. Forecast outputs are available at 1 h intervals. In this study, we used the 1–3 h lead-time forecasts to generate background profiles at 10 min intervals using time-weighted interpolation. Spatial interpolation was performed using an inverse-distance-weighting method based on the four nearest grid points to the observation site (KMA, 2013).

3.3 Radiative transfer model : RTTOV-gb

RTTOV-gb, used as the observation operator in this study, is a fast one-dimensional radiative transfer model (RTM) designed for ground-based upward-looking MWR observations and shares the same program interface as RTTOV (Cimini et al., 2019; De Angelis et al., 2016). The radiative transfer calculations employ the line-by-line absorption model developed by Rosenkranz (2017). When LDAPS profiles are provided as input, RTTOV-gb simulates TBs for 14 channels under clear-sky conditions. The Jacobian matrices are also computed using the RTTOV-gb K-module, which enables the iterative update in Eq. (3) within the 1D-VAR algorithm. RTTOV-gb has been shown to provide accurate MWR radiance simulations and physically consistent Jacobians (Cimini et al., 2019; De Angelis et al., 2016). Therefore, it is widely used as a forward model in data assimilation studies (Vural et al., 2024; Zheng et al., 2026). Within European profiling initiatives (Cimini et al., 2020; Illingworth et al., 2019), RTTOV-gb has been used for long-term observations-minus-background (O–B) monitoring of MWR networks (De Angelis et al., 2017). Martinet et al. (2020) applied RTTOV-gb within a 1D-VAR framework and demonstrated improved retrieval performance, further supporting its applicability in MWR-based retrieval systems.

3.4 Observation-error covariance matrix

In the 1D-VAR retrieval algorithm, the background and observation-error covariance matrices are used to weight the relative contributions of the background and the observations according to their uncertainties (Martinet et al., 2017). In previous studies, $\mathbf{R}$ was often approximated as a diagonal matrix (i.e., the off-diagonal elements were set to zero), based on the assumptions that observation errors were uncorrelated (Hewison, 2007; Martinet et al., 2017) and that systematic calibration errors were negligible or had been adequately corrected (Löhnert et al., 2004). However, in practice, residual observation errors may remain after bias correction and can be correlated across channels. Ikuta et al. (2025) reported strong inter-channel error correlations for a 14-channel MWR and noted that assimilating all channels while neglecting these correlations can degrade forecast accuracy. Therefore, in this study, after removing systematic biases, $\mathbf{R}$ was estimated to account for inter-channel error correlations.

https://doi.org/10.5194/egusphere-2026-3545
Preprint. Discussion started: 3 August 2026

The $\mathbf{R}$ consists of three components: radiometric noise from the instrument ($\mathbf{E}$), representativeness errors ($\mathbf{M}$), and radiative transfer model errors ($\mathbf{F}$). The instrumental noise term $\mathbf{E}$ can be estimated using TBs obtained during LN_2 calibration periods (Hewison, 2006). However, due to the limited availability of such calibration data, an alternative approach was adopted. Periods of continuously clear-sky conditions lasting at least 30 min during the IOPs were selected and assumed to represent sufficiently stable atmospheric conditions for calibration. Accordingly, $\mathbf{E}$ was estimated using the variance-covariance formulation, as defined by:

$$\mathbf{E} = (k-1)^{-1}\mathbf{y}'^{\mathrm{T}}\mathbf{y}', \tag{7}$$

where $\mathbf{y}'$ is a $k \times n$ matrix of TB anomalies with k observations and n channels (Wilks, 2011). This formulation corresponds to the sample covariance matrix method, which accounts for both the noise in each channel and inter-channel observation-error correlations to quantify the error. Under steady atmospheric conditions, variations in the observations are assumed to primarily represent instrument noise, allowing the variances and covariances to be empirically estimated.

NWP data are interpolated to the observation location, while the model fields are truncated in spatial and temporal scales compared with the true atmosphere. To account for this mismatch, the representativeness-error covariance matrix, $\mathbf{M}$, is added to the instrumental errors. $\mathbf{M}$ is defined as follows (Hewison, 2006):

$$\mathbf{M} = \varepsilon\,[(\boldsymbol{y}^0(t + \triangle t) - \boldsymbol{y}^0(t))(\boldsymbol{y}^0(t + \triangle t) - \boldsymbol{y}^0(t))^{\mathrm{T}}], \tag{8}$$

where $\boldsymbol{y}^0(t)$ and $\boldsymbol{y}^{\mathbf{0}}(t + \triangle t)$ denote observations separated by a time interval $\triangle t$, and ε represents the expectation operator. In this study, $\triangle t$ was set to 391 s, corresponding to the advection timescale across one 1.5 km LDAPS grid spacing using a representative wind speed of 3.8 $m\,s^{-1}$ during the IOPs. Observation differences over $\triangle t$ capture temporal variability and, implicitly, spatial representativeness errors, because the advection time corresponds to horizontal displacement on the model grid.

The radiative transfer model error, $\mathbf{F}$, primarily arises from spectroscopic uncertainties and differences among absorption models. Cimini et al. (2018) quantified the uncertainty of the absorption model used in microwave radiative transfer and calculated the corresponding uncertainty covariance matrix based on spectroscopic parameters. They also demonstrated that this covariance matrix can be directly applied in retrieval processes. Therefore, this study adopts the error covariance matrix proposed by Cimini et al. (2018) to account for errors in the radiative transfer model.

Table 1 shows the uncertainty of each channel, accounting for the three components of $\mathbf{R}$. The total observation-error covariance indicates large uncertainties at 51.26 and 52.28 GHz, mainly due to $\mathbf{F}$ associated with uncertainty in the O_2 absorption model. In the 26–54 GHz range, $\mathbf{F}$ is the dominant contributor, whereas above 54 GHz, $\mathbf{M}$ contributes more substantially. Hewison (2006) reported that $\mathbf{E}$ is the dominant contributor in the highest frequency channels, while $\mathbf{M}$ is more important in channels sensitive to cloud. This discrepancy may arise from differences in the RTM configuration and in the spatiotemporal variability represented in the NWP.

The correlation matrix (Fig. 4) shows strong inter-channel observation-error correlations among the K-band channels, and similarly strong correlations within the more transparent V-band channels. This suggests that a substantial fraction of the

https://doi.org/10.5194/egusphere-2026-3545
Preprint. Discussion started: 3 August 2026

observation-error variability is shared across nearby channels, reflecting common error sources such as representativeness and forward model errors.

Table 1. Diagonal elements of the observation-error covariance matrix (R) for each channel, showing the contributions from instrument noise (E), forward model error (F), and representativeness error (M), together with the total uncertainty.

Frequency (GHz)	Instrument noise E [K]	Radiative transfer model error F [K]	Representativeness error M [K]	Total uncertainty R [K]
22.24	0.33	0.46	0.39	0.69
23.04	0.32	0.42	0.38	0.65
23.84	0.28	0.37	0.33	0.57
25.44	0.20	0.34	0.23	0.46
26.24	0.17	0.34	0.20	0.43
27.84	0.14	0.36	0.17	0.42
31.40	0.14	0.42	0.17	0.48
51.26	0.45	2.86	0.65	2.97
52.28	0.44	3.04	0.63	3.14
53.86	0.42	1.12	0.60	1.33
54.94	0.45	0.14	0.64	0.80
56.66	0.33	0.02	0.47	0.57
57.30	0.30	0.02	0.42	0.52
58.00	0.25	0.02	0.35	0.44

https://doi.org/10.5194/egusphere-2026-3545
Preprint. Discussion started: 3 August 2026

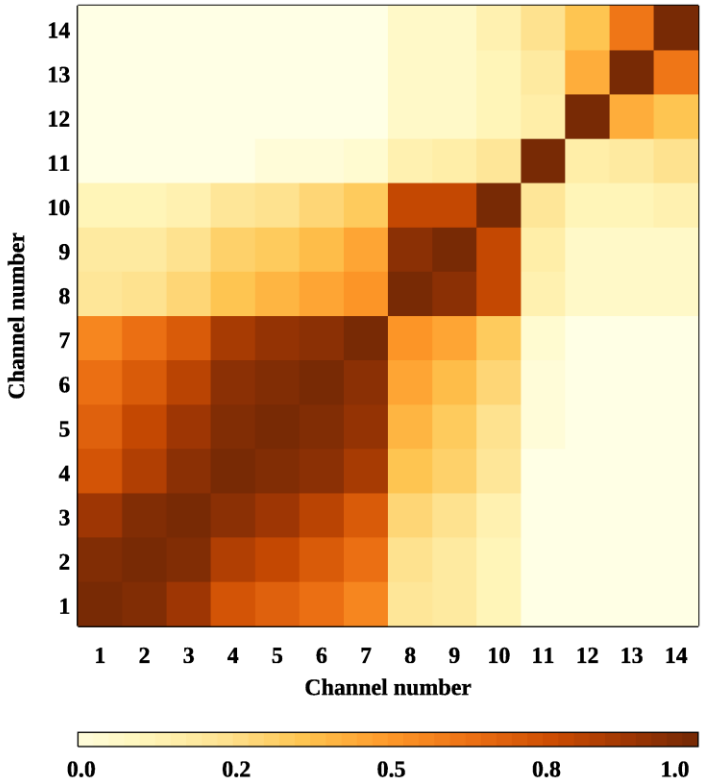

255 **Figure 4: Inter-channel observation-error correlation matrix derived from the observation-error covariance matrix (R) for the 14-channel MWR.**

3.5 Background-error covariance matrix

The background-error covariance matrix, $\mathbf{B}$, specifies how much weight is given to the a priori profile relative to the observations. It plays a crucial role in the retrieval because it ensures balance among variables in NWP models (Martinet et al., 2020), assigns weights to the background, and adjusts increments to derive the solution. In this study, $\mathbf{B}$ is obtained from statistical background-error estimates for each level of temperature, humidity, and surface temperature from the UM-based background profile, interpolated to the 101 levels used in the observation operator.

https://doi.org/10.5194/egusphere-2026-3545
Preprint. Discussion started: 3 August 2026

4 Results

4.1 Retrieval performance of the 1D-VAR system

To evaluate the retrieval performance, the RMSE and bias of the O–B departures are compared with those of the observation minus the simulated TB derived from the 1D-VAR retrieval output (O–R). The RMSE of O–B reaches up to 2.6 K, whereas that of O–R does not exceed 0.8 K, with all channels showing lower RMSEs for O–R than for O–B. The reduction is particularly pronounced for the K-band channels near the centre of the water vapor absorption line, where large initial discrepancies are substantially reduced. A slight increase in mean bias (MB) of O–R is observed, particularly in channels sensitive to water vapor, which are more strongly influenced by the background. Figure 5 depicts histograms of O–B and O–R for the study period. Panels (a) and (b) correspond to water vapor sensitive channels at K-band, whereas panels (c) and (d) show oxygen sensitive channels at V-band. Each panel includes skewness and full width at half maximum (FWHM). Skewness quantifies the asymmetry of a distribution, with positive or negative values indicating the direction of skewness, and its absolute value indicates its magnitude. The skewness of O–B is predominantly positive across most channels associated with large departures from the background. After retrieval, the skewness of O–R is reduced, indicating that the retrieval effectively suppresses large positive departures and leads to a more symmetric error distribution centered around zero. O–R exhibits a smaller FWHM than O–B, indicating a narrower spread and reduced variability. A Kolmogorov–Smirnov test at the 5 % significance level indicates statistically significant differences between the O–B and O–R distributions for each channel. Overall, these results suggest that the retrieval reduces TB departures and yields consistent behavior across channels, supporting the robustness of the retrieval system.

https://doi.org/10.5194/egusphere-2026-3545
Preprint. Discussion started: 3 August 2026

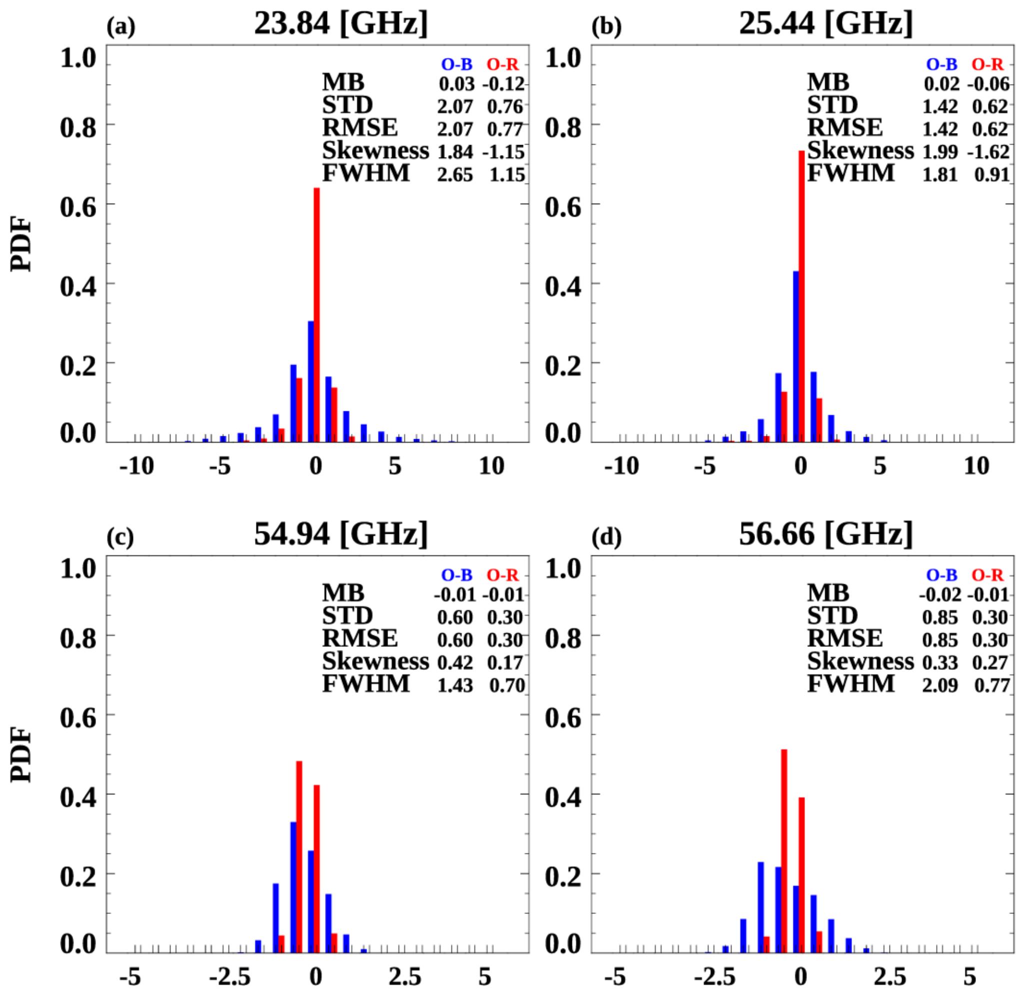

Figure 5: Histograms of TB departures for O–B (blue) and O–R (red) over the study period for (a) 23.84 GHz, (b) 27.84 GHz, (c) 54.94 GHz and (d) 56.66 GHz.

4.2 Validation of retrieved profiles

The 1D-VAR retrievals were validated against radiosondes from 137 launches during the IOPs; clear-sky conditions were met in 41 cases, and the results were compared with those from the background and the manufacturer-provided neural network (NN) retrievals. The NN retrievals were computed using the internal HATPRO MWR software from TBs without bias correction, whereas the 1D-VAR retrievals were based on bias-corrected TBs.

https://doi.org/10.5194/egusphere-2026-3545
Preprint. Discussion started: 3 August 2026

During the validation periods, 41 1D-VAR retrievals were matched with radiosondes. Figure 6 presents the RMSE and bias of the 1D-VAR retrievals (red), NN retrievals (black), and background (blue), each calculated relative to the radiosondes.

In the temperature validation, both the 1D-VAR retrievals and the background exhibit negative biases, underestimating temperatures compared to the radiosonde. The largest negative bias (–1.07 K) is found in the background near the surface, while the smallest bias, close to zero, is observed around 1,550 m for both the background and the 1D-VAR retrievals. The NN retrievals also display negative biases at all altitudes, decreasing from the surface to about 230 m, and then gradually increasing with height. The negative bias probably originates from spectroscopic biases in the absorption models (Cimini et al., 2006).

The RMSE of the 1D-VAR retrievals gradually decreases with height up to approximately 400 m (to 1.04 K), reaches a maximum of 1.32 K at around 800 m, indicating a height-dependent variation in retrieval performance. The NN retrievals have an RMSE of 1.49 K near the surface, which increases with height to about 3.1 K. Conversely, the background RMSE increases toward the surface, with the largest value (1.73 K) in the lowest layer.

The accuracy of the 1D-VAR retrievals is similar to that of the NN retrievals from the surface to 1000 m, whereas above this altitude, it more closely matches the performance of the background. These results are consistent with Martinet et al. (2015). The overall RMSE of the 1D-VAR temperature retrievals is 1 K, which is lower than that of the background (1.15 K), representing an improvement of approximately 23 % below 1000 m and 12 % across all altitudes. This indicates that the 1D-VAR retrievals provide most of the information in the lower atmospheric layers.

For the RMSE of humidity profiles, the NN retrievals showed larger values than other profiles, particularly in the lower layer. The 1D-VAR retrieval and background exhibited similar trends. The 1D-VAR retrieval demonstrated a slight improvement over the background. Although the rate of error reduction was lower than that for temperature, the maximum reduction reaches approximately 0.2 $g\,kg^{-1}$ at 720 m (with a bias of 0.14 $g\,kg^{-1}$ at 530 m). Overall, the RMSE of the 1D-VAR humidity retrievals showed a 9 % improvement compared to the background, including a 12 % improvement in the lower layer.

The 1D-VAR retrieval estimates the optimal atmospheric state by combining MWR observations and the background. The retrieval was strongly influenced by the MWR in the lower layers, whereas it relies more heavily on the background above 1000 m. The radiosonde validation confirmed that the 1D-VAR retrieval outperforms the background below 1000 m, particularly for the temperature profiles.

https://doi.org/10.5194/egusphere-2026-3545
Preprint. Discussion started: 3 August 2026

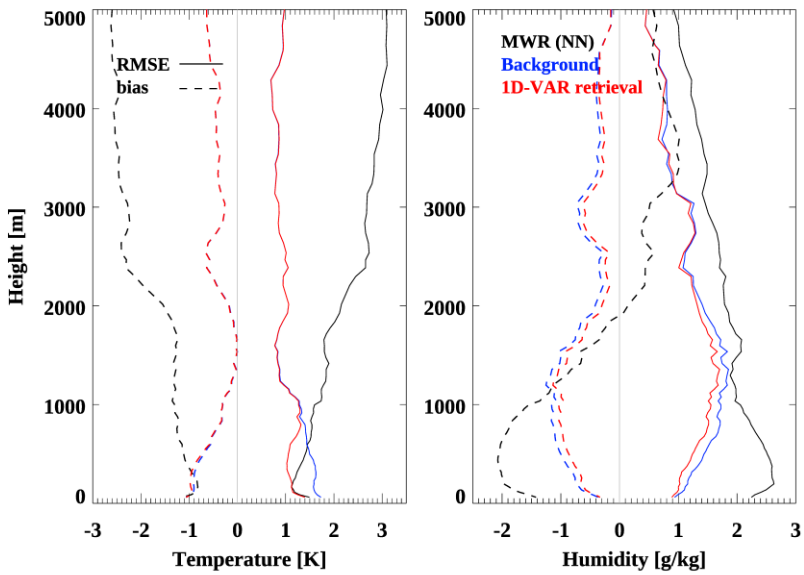

Figure 6: Vertical profiles of RMSE (solid lines) and bias (dashed lines) for temperature and humidity, comparing the 1D-VAR retrievals (red), background profiles (blue), and MWR neural network retrievals (black) relative to radiosondes during the IOPs.

4.3 Impact of correlated observation-error covariance matrix

The correlated observation-error covariance matrix (FULL) reflects a more realistic error structure than the diagonal observation-error covariance matrix (DIAG) and can improve retrieval performance. To assess the impact of using FULL in the 1D-VAR system, we compared the results with those obtained using DIAG, in which only the diagonal elements of the FULL are retained and all off-diagonal elements are set to zero. Using the quality-controlled set of 24 312 observations, both configurations achieved near-identical success rates. FULL converged faster among successful retrievals. About 5.7 % of successful cases terminated after a single iteration, while most terminated after two iterations, and the remainder converged by the third iteration. In contrast, the corresponding fraction for DIAG was only 0.1 %; most successful DIAG retrievals required two iterations, and a few cases needed up to six iterations. In addition, the FULL configuration reduced the total elapsed processing time (real time) from 83 min 17.880 s to 81 min 8.708 s in our benchmark run, indicating a modest computational efficiency gain (about 2.6 %). These results indicate that accounting for inter-channel observation-error correlations improves convergence efficiency.

In the validation against radiosonde observations during the IOPs (41 cases, clear-sky), all retrieved profiles were closer to the radiosonde observations than the NWP background. FULL showed smaller errors than DIAG, with the largest temperature

https://doi.org/10.5194/egusphere-2026-3545
Preprint. Discussion started: 3 August 2026

difference (0.22 K) occurring at 677 m within the transition layer between the developing mixed layer and the residual layer. For humidity, the maximum difference of 0.54 $g\ kg^{-1}$ occurs at 4800 m under dry atmospheric conditions.

Statistically, FULL further reduced the RMSE by 1.02 % for temperature and 4.52 % for humidity below 1000 m with respect to DIAG. However, DIAG showed slightly lower temperature RMSE between 400 m and 1000 m (Fig. 7). To investigate this, an additional experiment was conducted where the inter-channel correlations among the V-band temperature channels were weakened by scaling the off-diagonal elements to 0.05, which was found to be the optimal threshold in this study (FULL.wt). Consequently, while the temperature RMSE of FULL.wt increased slightly below 400 m, it showed consistently improved performance compared with DIAG below 1000 m. These results are consistent with the physical characteristics of the Jacobians. For channels above 54 GHz, the weighting functions exhibit strong peaks below 400 m, where the observational signal is dominant. Therefore, the temperature RMSE is minimized by effectively reducing observational noise using inter-channel error correlations.

Meanwhile, the Jacobians overlap between 400 m and 1000 m, indicating relatively weak sensitivity. This suggests that the FULL may, in this layer, down-weight overlapping information, which may lead to a slight reduction in the actual atmospheric signal. By adjusting the inter-channel correlation weighting (FULL.wt), the noise-removal effect in the lowest layer is preserved, while signal loss in the transition layer is mitigated, thereby achieving optimized retrieval performance across all altitudes.

In humidity retrievals, the use of correlated information yields larger improvements than in temperature retrievals. This can be attributed to the vertically broad distribution and similar shapes of the humidity Jacobians, which enhance the effectiveness of inter-channel information. These results indicate that the FULL configuration consistently yields lower bias and RMSE than DIAG up to 3000 m. Based on these findings, FULL.wt is adopted in the following analyses and is hereafter referred to as FULL unless otherwise stated.

https://doi.org/10.5194/egusphere-2026-3545
Preprint. Discussion started: 3 August 2026

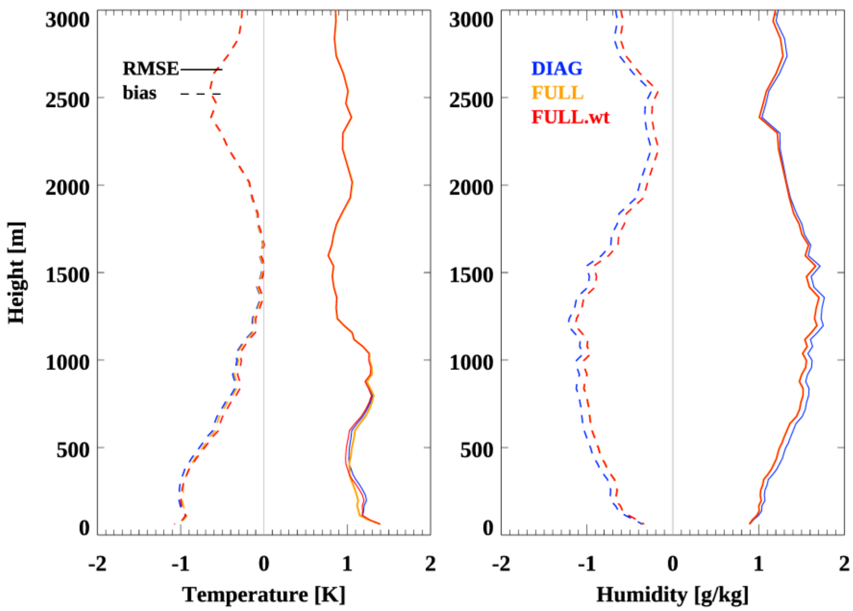

Figure 7: Vertical profiles of RMSE (solid lines) and bias (dashed lines) for temperature and humidity, comparing the 1D-VAR retrievals of DIAG (blue), FULL (orange), and FULL.wt (red), all relative to radiosondes during the IOPs.

4.4 Case study

In this section, the 1D-VAR retrieval outputs are analyzed in the context of temporal atmospheric changes observed during the IOPs on 22–23 September 2016. During this event, the convective mixed layer developed up to 2,000 m by 15 LST on 22 September following sunrise. After sunset (18 LST), temperatures in the lower atmosphere decreased due to surface cooling, and a stable layer formed and deepened to about 500 m by 03 LST on 23 September. With the onset of sunrise, surface heating from solar radiation initiated the development of unstable atmospheric conditions.

Figure 8 presents the time series of temperature-difference profiles for (a) background minus radiosonde and (b) 1D-VAR retrieval minus radiosonde. From 15 to 21 LST on 22 September, the background exhibits a relatively positive bias below 1000 m under convective conditions. Following sunset, the boundary layer transitions toward stable conditions, and the background bias shifts to negative values and becomes increasingly pronounced, indicating an underestimation of the nighttime cooling structure in the lower layer. After sunrise (06 LST on 23 September), the strong negative bias (Fig. 8a) further suggests that the background fails to capture daytime warming, with a maximum difference of approximately –4.16 K around 400 m at 09 LST.

https://doi.org/10.5194/egusphere-2026-3545
Preprint. Discussion started: 3 August 2026

At 15 LST on 22 September, when the background shows a positive bias, the 1D-VAR retrieval exhibits an opposite bias under unstable conditions with a slightly larger magnitude. After 21 LST, the 1D-VAR retrieval generally reduces the magnitude of the lower-tropospheric biases. The FULL configuration reduces this bias more effectively than the DIAG configuration, with a maximum reduction of 38 %. During the evening-to-nocturnal stabilization and the subsequent morning redevelopment, the negative bias of the 1D-VAR retrieval remains relatively small below 1000 m, indicating that it captures near-surface variability of the evolving boundary layer structure better than background.

Around 2000 m, both profiles show the same bias direction and similar magnitudes of temperature differences. In the upper layer, the temperature differences remain similar to those of the background, reflecting the strong dependence of the retrieval on the background. These results indicate that the 1D-VAR retrieval effectively reproduces temperature changes in the lower layer, consistent with the substantial error reduction below 1000 m shown in Fig. 6.

In contrast to temperature, the humidity difference profiles for the background and the 1D-VAR retrieval are generally similar. Below 2500 m, most profiles exhibit a negative bias, indicating an underestimation compared to the radiosonde. Large negative biases appear on 23 September, with the magnitude of the bias in the 1D-VAR retrieval being smaller than that in the background. Unlike the time series of temperature differences, where the 1D-VAR retrieval shows substantial improvement in the lower layer, the humidity bias remains negative across time and altitude, although its magnitude varies.

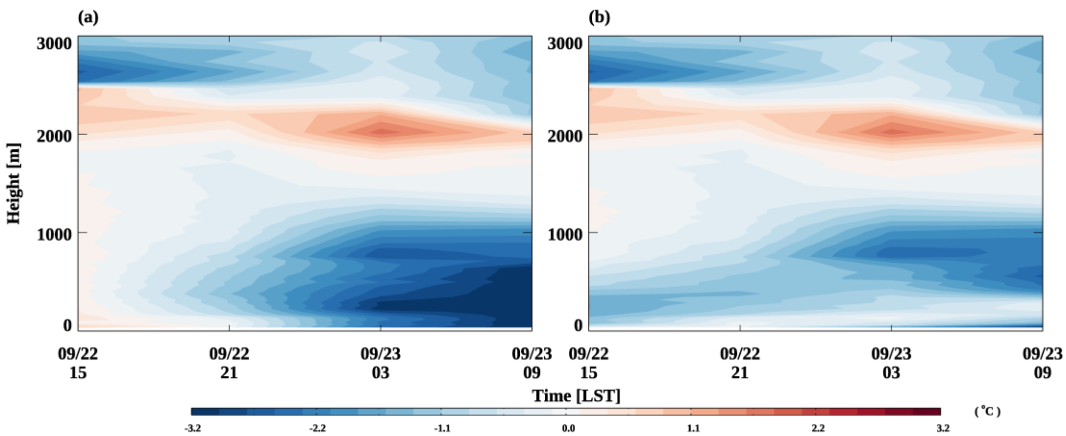

Figure 8: Time series of temperature differences on 22-23 September: (a) background minus radiosonde, and (b) 1D-VAR retrieval minus radiosonde.

5. Summary and Conclusions

This study developed and evaluated a clear-sky 1D-VAR retrieval system for ground-based MWR observations at the Jungnang site in Seoul during 2015–2016, and examined the impact of incorporating inter-channel observation-error correlations into the observation-error covariance matrix on retrieval performance. In the first part, QC was implemented through clear-sky screening and O–B monitoring to ensure that the assumptions required for 1D-VAR retrievals were met. Because K-band channels are sensitive to clouds and precipitation, a cloud detection algorithm and the TB variability at 31.4 GHz were used to remove cloudy cases and exclude rain-flagged data. For V-band channels, discontinuities in O–B were observed after LN_2 calibration due to water condensation on the aluminum plate reflector and radiometer radome, as well as a non-homogeneous coverage of the absorber with LN_2, which hindered retrieval convergence. To mitigate these effects, systematic bias correction was applied within each calibration interval. As a result, biased data were removed, and outliers better satisfied the 1D-VAR assumptions.

The second part focused on configuring the 1D-VAR system and specifying the observation-error covariance matrix (**R**). Using samples derived from bias-corrected, clear-sky MWR observations during the IOPs, we derived a correlated **R** that represents inter-channel error correlations. In the 26–54 GHz range, **F** is the dominant contributor, whereas above 54 GHz, **M** becomes dominant. The total uncertainties reach their maximum near 51–52 GHz. The correlation structure indicated strong relationships among K-band channels and among the more transparent V-band channels.

In the third part, retrieval performance for the FULL configuration was evaluated. For all channels, the O–R RMSEs were lower than the O–B RMSEs, with particularly pronounced reductions at 22.24 GHz. In addition, the O–R residual distributions were closer to Gaussian, indicating stable retrieval behavior. Radiosonde validation showed that the 1D-VAR retrievals outperformed LDAPS background below 1000 m, reducing temperature RMSE by up to 23 % and humidity RMSE by about 12 %.

To further evaluate the impact of inter-channel error correlations, we performed a direct comparison between FULL and its diagonal counterpart, DIAG. In this comparison, FULL increased the fraction of one-iteration retrievals (5.7 % compared with 0.1 %) and reduced the total elapsed runtime by 2.6 % in our benchmark run. In radiosonde validations, FULL outperformed DIAG, reducing the RMSE by 1.02 % for temperature and 4.52 % for humidity below 1000 m. However, for temperatures between 400 m and 1000 m, FULL misinterpreted effective channel signals as noise, resulting in a larger RMSE than DIAG. By scaling the off-diagonal elements of V-band channels to 0.05, the algorithm consistently improved temperature retrieval performance below 1000 m while maintaining humidity accuracy.

In summary, the developed clear-sky 1D-VAR system effectively utilizes MWR observations to enhance lower-tropospheric thermodynamic profiling. The retrieved profiles captured near-surface variability and better represented boundary-layer transition processes than the background. Explicitly accounting for inter-channel observation-error correlations primarily improves numerical stability and convergence efficiency, while also improving radiosonde-validated accuracy. Future work will incorporate low-elevation angle TB observations and extend the framework to a wider range of weather conditions beyond clear-sky cases to further improve robustness and applicability.

https://doi.org/10.5194/egusphere-2026-3545
Preprint. Discussion started: 3 August 2026

Code and data availability

RTTOV-gb is available from the NWP SAF under its licensing conditions. The 1D-VAR retrieval code and observation data used in this study are available upon reasonable request from the corresponding author. LDAPS data are available from the Korea Meteorological Administration (KMA) through the KMA API Hub.

Author contributions

MHA conceptualized and supervised the study. YS developed the 1D-VAR algorithm, conducted the research, and prepared the manuscript. SJL contributed to the development of the retrieval algorithm and the review and editing of the manuscript. DC contributed to the application of RTTOV-gb and reviewed the manuscript. CKS contributed to the analyses presented in Sects. 3.4 and 4.3. All authors contributed to the revision of the manuscript.

Competing interests

One of the (co-)authors is a member of the editorial board of Atmospheric Measurement Techniques.

Financial support

This work was funded by the Korea Meteorological Administration Research and Development Program under Grant (RS-2025-02221093).

References

Ahn, M.-H., Han, D., Won, H. Y., and Morris, V.: A cloud detection algorithm using the downwelling infrared radiance measured by an infrared pyrometer of the ground-based microwave radiometer, Atmos. Meas. Tech., 8, 553–566, https://doi.org/10.5194/amt-8-553-2015, 2015.

Byon, J.-Y., Hong, S.-O., Park, Y.-S., and Kim, Y.-H.: Evaluation of the Urban Heat Island Intensity in Seoul Predicted from KMA Local Analysis and Prediction System, J. Korean Earth Sci. Soc., 42, 135–148, https://doi.org/10.5467/JKESS.2021.42.2.135, 2021.

Calaf, M., Vercauteren, N., Katul, G. G., Giometto, M. G., Morrison, T. J., Margairaz, F., Boyko, V., and Pardyjak, E. R.: Boundary-Layer Processes Hindering Contemporary Numerical Weather Prediction Models, Boundary-Layer Meteorol, 186, 43–68, https://doi.org/10.1007/s10546-022-00742-5, 2023.

Cimini, D., Westwater, E. R., Yong Han, and Keihm, S. J.: Accuracy of ground-based microwave radiometer and balloon-borne measurements during the WVIOP2000 field experiment, IEEE Trans. Geosci. Remote Sensing, 41, 2605–2615, https://doi.org/10.1109/TGRS.2003.815673, 2003.

Cimini, D., Hewison, T. J., Martin, L., Güldner, J., Gaffard, C., and Marzano, F. S.: Temperature and humidity profile retrievals from ground-based microwave radiometers during TUC, metz, 15, 45–56, https://doi.org/10.1127/0941-2948/2006/0099, 2006.

Cimini, D., Westwater, E. R., and Gasiewski, A. J.: Temperature and Humidity Profiling in the Arctic Using Ground-Based Millimeter-Wave Radiometry and 1DVAR, IEEE Trans. Geosci. Remote Sensing, 48, 1381–1388, https://doi.org/10.1109/TGRS.2009.2030500, 2010.

Cimini, D., Campos, E., Ware, R., Albers, S., Giuliani, G., Oreamuno, J., Joe, P., Koch, S. E., Cober, S., and Westwater, E.: Thermodynamic Atmospheric Profiling During the 2010 Winter Olympics Using Ground-Based Microwave Radiometry, IEEE Trans. Geosci. Remote Sensing, 49, 4959–4969, https://doi.org/10.1109/TGRS.2011.2154337, 2011.

Cimini, D., Rosenkranz, P. W., Tretyakov, M. Y., Koshelev, M. A., and Romano, F.: Uncertainty of atmospheric microwave absorption model: impact on ground-based radiometer simulations and retrievals, Atmos. Chem. Phys., 18, 15231–15259, https://doi.org/10.5194/acp-18-15231-2018, 2018.

Cimini, D., Hocking, J., De Angelis, F., Cersosimo, A., Di Paola, F., Gallucci, D., Gentile, S., Geraldi, E., Larosa, S., Nilo, S., Romano, F., Ricciardelli, E., Ripepi, E., Viggiano, M., Luini, L., Riva, C., Marzano, F. S., Martinet, P., Song, Y. Y., Ahn, M. H., and Rosenkranz, P. W.: RTTOV-gb v1.0 – updates on sensors, absorption models, uncertainty, and availability, Geosci. Model Dev., 12, 1833–1845, https://doi.org/10.5194/gmd-12-1833-2019, 2019.

Cimini, D., Haeffelin, M., Kotthaus, S., Löhnert, U., Martinet, P., O'Connor, E., Walden, C., Coen, M. C., and Preissler, J.: Towards the profiling of the atmospheric boundary layer at European scale—introducing the COST Action PROBE, Bull. of Atmos. Sci.& Technol., 1, 23–42, https://doi.org/10.1007/s42865-020-00003-8, 2020.

De Angelis, F., Cimini, D., Hocking, J., Martinet, P., and Kneifel, S.: RTTOV-gb – adapting the fast radiative transfer model RTTOV for theassimilation of ground-based microwave radiometer observations, Geosci. Model Dev., 9, 2721–2739, https://doi.org/10.5194/gmd-9-2721-2016, 2016.

De Angelis, F., Cimini, D., Löhnert, U., Caumont, O., Haefele, A., Pospichal, B., Martinet, P., Navas-Guzmán, F., Klein-Baltink, H., Dupont, J.-C., and Hocking, J.: Long-term observations minus background monitoring of ground-based brightness temperatures from a microwave radiometer network, Atmos. Meas. Tech., 10, 3947–3961, https://doi.org/10.5194/amt-10-3947-2017, 2017.

Desroziers, G., Berre, L., Chapnik, B., and Poli, P.: Diagnosis of observation, background and analysis-error statistics in observation space, Quart J Royal Meteoro Soc, 131, 3385–3396, https://doi.org/10.1256/qj.05.108, 2005.

Ebell, K., Löhnert, U., Päschke, E., Orlandi, E., Schween, J. H., and Crewell, S.: A 1-D variational retrieval of temperature, humidity, and liquid cloud properties: Performance under idealized and real conditions, JGR Atmospheres, 122, 1746–1766, https://doi.org/10.1002/2016JD025945, 2017.

Hewison, T.: Profiling Temperature and Humidity by Ground-based Microwave Radiometers, PhD Thesis, University of Reading, Reading, UK, 2006.

Hewison, T. J.: 1D-VAR Retrieval of Temperature and Humidity Profiles From a Ground-Based Microwave Radiometer, IEEE Trans. Geosci. Remote Sensing, 45, 2163–2168, https://doi.org/10.1109/TGRS.2007.898091, 2007.

Hewison, T. J., Wu, X., Yu, F., Tahara, Y., Hu, X., Kim, D., and Koenig, M.: GSICS Inter-Calibration of Infrared Channels of Geostationary Imagers Using Metop/IASI, IEEE Trans. Geosci. Remote Sensing, 51, 1160–1170, https://doi.org/10.1109/TGRS.2013.2238544, 2013.

Hu, G. and Dance, S. L.: Sampling and misspecification errors in the estimation of observation-error covariance matrices using observation-minus-background and observation-minus-analysis statistics, Quart J Royal Meteoro Soc, 150, 3052–3077, https://doi.org/10.1002/qj.4750, 2024.

Ikuta, Y., Seko, H., Yoshimoto, K., Yamamoto, K., Kawabata, T., Ishimoto, H., Araki, K., Tajiri, T., and Shimizu, S.: Impact of direct assimilation of ground-based microwave radiometer on numerical weather prediction: Accounting for interchannel observation error correlations, Quart J Royal Meteoro Soc, 151, e5067, https://doi.org/10.1002/qj.5067, 2025.

Illingworth, A. J., Cimini, D., Haefele, A., Haeffelin, M., Hervo, M., Kotthaus, S., Löhnert, U., Martinet, P., Mattis, I., O'Connor, E. J., and Potthast, R.: How Can Existing Ground-Based Profiling Instruments Improve European Weather Forecasts?, Bulletin of the American Meteorological Society, 100, 605–619, https://doi.org/10.1175/BAMS-D-17-0231.1, 2019.

Kang, M., Lim, Y.-K., Cho, C., Kim, K. R., Park, J. S., and Kim, B.-J.: The Sensitivity Analyses of Initial Condition and Data Assimilation for a Fog Event using the Mesoscale Meteorological Model, J. Korean Earth Sci. Soc., 36, 567–579, https://doi.org/10.5467/JKESS.2015.36.6.567, 2015.

Kim, D.-J., Kang, G., Kim, D.-Y., and Kim, J.-J.: Characteristics of LDAPS-Predicted Surface Wind Speed and Temperature at Automated Weather Stations with Different Surrounding Land Cover and Topography in Korea, Atmosphere, 11, 1224, https://doi.org/10.3390/atmos11111224, 2020.

Korea Meteorological Administration (KMA): Numerical Weather Prediction Supports the Weather and Climate Industry: A Guide to the Utilization of Numerical Weather Prediction Model Data., Korea Meteorological Administration (KMA), 2013.

Löhnert, U. and Maier, O.: Operational profiling of temperature using ground-based microwave radiometry at Payerne: prospects and challenges, Atmos. Meas. Tech., 5, 1121–1134, https://doi.org/10.5194/amt-5-1121-2012, 2012.

Löhnert, U., Crewell, S., and Simmer, C.: An Integrated Approach toward Retrieving Physically Consistent Profiles of Temperature, Humidity, and Cloud Liquid Water, J. Appl. Meteor., 43, 1295–1307, https://doi.org/10.1175/1520-0450(2004)043%3C1295:AIATRP%3E2.0.CO;2, 2004.

Martinet, P., Dabas, A., Donier, J.-M., Douffet, T., Garrouste, O., and Guillot, R.: 1D-Var temperature retrievals from microwave radiometer and convective scale model, Tellus A: Dynamic Meteorology and Oceanography, 67, 27925, https://doi.org/10.3402/tellusa.v67.27925, 2015.

https://doi.org/10.5194/egusphere-2026-3545
Preprint. Discussion started: 3 August 2026

Martinet, P., Cimini, D., De Angelis, F., Canut, G., Unger, V., Guillot, R., Tzanos, D., and Paci, A.: Combining ground-based microwave radiometer and the AROME convective scale model through 1DVAR retrievals in complex terrain: an Alpine valley case study, Atmos. Meas. Tech., 10, 3385–3402, https://doi.org/10.5194/amt-10-3385-2017, 2017.

Martinet, P., Cimini, D., Burnet, F., Ménétrier, B., Michel, Y., and Unger, V.: Improvement of numerical weather prediction model analysis during fog conditions through the assimilation of ground-based microwave radiometer observations: a 1D-Var study, Atmos. Meas. Tech., 13, 6593–6611, https://doi.org/10.5194/amt-13-6593-2020, 2020.

Martinet, P., Bell, A., Caumont, O., Vié, B., Burnet, F., and Delanoë, J.: Optimal estimation of thermodynamic and microphysical profiles within fog events from ground-based microwave radiometer and cloud radar synergy, EGU General Assembly 2022, Vienna, Austria, 23–27 May 2022, EGU22-12410, https://doi.org/10.5194/egusphere-egu22-12410, 2022.

Powers, J. G., Klemp, J. B., Skamarock, W. C., Davis, C. A., Dudhia, J., Gill, D. O., Coen, J. L., Gochis, D. J., Ahmadov, R., Peckham, S. E., Grell, G. A., Michalakes, J., Trahan, S., Benjamin, S. G., Alexander, C. R., Dimego, G. J., Wang, W., Schwartz, C. S., Romine, G. S., Liu, Z., Snyder, C., Chen, F., Barlage, M. J., Yu, W., and Duda, M. G.: The Weather Research and Forecasting Model: Overview, System Efforts, and Future Directions, Bulletin of the American Meteorological Society, 98, 1717–1737, https://doi.org/10.1175/BAMS-D-15-00308.1, 2017.

Rodgers, C. D.: Inverse methods for atmospheric sounding: theory and practice, World Scientific, Singapore, 2000.

Rosenkranz, P. W.: Line-by-line microwave radiative transfer (non-scattering), Remote Sens. Code Library, https://doi.org/10.21982/M81013, 2017.

Stewart, L. M., Dance, S. L., and Nichols, N. K.: Correlated observation errors in data assimilation, Numerical Methods in Fluids, 56, 1521–1527, https://doi.org/10.1002/fld.1636, 2008.

Stewart, L. M., Dance, S. L., and Nichols, N. K.: Data assimilation with correlated observation errors: experiments with a 1-D shallow water model, Tellus A: Dynamic Meteorology and Oceanography, 65, 19546, https://doi.org/10.3402/tellusa.v65i0.19546, 2013.

Thomas, G., Martinet, P., Brousseau, P., Chambon, P., Georgis, J., Hervo, M., Huet, T., Löhnert, U., Orlandi, E., and Unger, V.: Assimilation of Ground-Based Microwave Radiometer Temperature Observations Into a Convective-Scale NWP Model for Fog Forecast Improvement, Quart J Royal Meteoro Soc, 151, e4893, https://doi.org/10.1002/qj.4893, 2025.

Vural, J., Merker, C., Löffler, M., Leuenberger, D., Schraff, C., Stiller, O., Schomburg, A., Knist, C., Haefele, A., and Hervo, M.: Improving the representation of the atmospheric boundary layer by direct assimilation of ground-based microwave radiometer observations, Quart J Royal Meteoro Soc, 150, 1012–1028, https://doi.org/10.1002/qj.4634, 2024.

Weston, P. P., Bell, W., and Eyre, J. R.: Accounting for correlated error in the assimilation of high-resolution sounder data, Quart J Royal Meteoro Soc, 140, 2420–2429, https://doi.org/10.1002/qj.2306, 2014.

Wilks, D. S.: Statistical methods in the atmospheric sciences, 3rd ed., Academic Press, Oxford Waltham, MA, 2011.

Zheng, Q., Sun, W., Liu, Z., Mao, J., He, J., Li, J., and Jiang, X.: Direct assimilation of ground-based microwave radiometer observations with machine learning bias correction based on developments of RTTOV-gb v1.0 and WRFDA v4.5, Geosci. Model Dev., 19, 731–754, https://doi.org/10.5194/gmd-19-731-2026, 2026.